Numerical simulation of impact and lift–off events in the hydrostatic skeleton of the leech

Christian Alscher

Department of Mathematics, University of Bielefeld

P.O. Box 100131, 33615 Bielefeld, Germany

email: alscher@mathematik.uni-bielefeld.de

Abstract In this paper we present a mechanical model of the hydrostatic skeleton and simulate the collision with an obstacle. The model is based on the worm–like shape of the medicinal leech and consists of a sequence of hexahedral segments with elastic edges and constant internal volume. Lagrange's equations of motion with holonomic constraints for the volume lead to a differential–algebraic system (DAE). The contact of the model with an obstacle including tangential friction is realized by Coulomb's law, this leads to unilateral constraints in the system. A switching algorithm is set up to detect impact and lift–off events as well as sliding/sticking transitions during contact. In periods of smooth motion the DAE system is solved by semi–explicit numerical methods implemented in the code MEXAX.

1 Introduction

The constructional principle of the hydrostatic (or fluid) skeleton is found in many soft–bodied animals as well as in reptilian tongues, tentacles of squid, and trunks of elephants, see e.g. [7], [21], [35], [36]. In physical terms, it is realized as an incompressible fluid enclosed by an elastic body wall. Contraction or relaxation of muscles embedded in the body wall leads to changes in the shape of the body by means of a pressure applied to the internal fluid. In 1950 Garth Chapman discussed the basic biomechanical principles of antagonistic muscle activation in hydrostatic skeletons in an intuitive way (see [6]), and in order to get an integrative insight in the complex functioning a simulation–based approach was chosen in [37] as well as in [7] and [32]. We consider a specific animal, the medicinal leech (*Hirudo medicinalis L.*). Much is already known about its morphology, the structure of its nervous system, and the neuronal control of muscles

during motions like swimming and crawling (see e.g. [24], [33]). However, the interaction of muscle activity and the complex functioning of the body during the motion can only be studied in a simulation–based approach. The dynamic model consists of a sequence of hexahedral segments with lumped masses in the corners and damped elastic springs as edges. The relation between length, tension, and velocity in these elastic elements represents the viscoelastic properties of the muscles. The system is stabilized by the constraint of constant volume either in the whole body or in prescribed compartments, and the equations of motion lead to a DAE system for the mass–points in the corners. In this paper, we restrict the mobility of the model by an obstacle, this leads to additional unilateral constraints. Each mass–point in the system is either distant from the obstacle (passive) or in contact with the obstacle (active) and we find a unilateral constraint for the relative distance. Furthermore, in a non–adhesive contact situation there is a contact force acting in the direction of the outward normal of the obstacle. It has to vanish as soon as the mass–point lifts off and this leads to a unilateral constraint for the contact force. These two unilateral constraints of "no penetration" and "no adhesion" are connected by a complementarity condition that is added to the DAE system. During the motion some mass–points might collide with the obstacle or lift off, this leads to jump discontinuities in the solution.

We consider the DAE system with all active constraints and solve the system numerically by the extrapolation code MEXAX (see [11], [27], [28]). A modified half–explicit Euler method is used to discretize the equations on velocity level and projections ensure the original constraints on position level. We set up a switching algorithm with a constraint addition–deletion technique (see [15]), where roots of switching functions indicate a collision or a lift–off. If such an event occurs the integration is interrupted, the corresponding constraint is added or deleted, and new initial values are determined by jump conditions and "hidden" constraints. Furthermore, for all active constraints the switching algorithm accounts for the transitions from sticking to sliding friction using Coulomb's law.

2 The dynamic model

The model consists of N connected hexahedral segments with $d = 4N+4$ corners, elastic edges, and constant total volume, see Fig. 1. The elastic edges resemble the longitudinal and circular musculature of the hydrostatic skeleton of the leech. There are longitudinal and circular elastic elements (LEs and CEs). The dorsoventral muscles of the leech

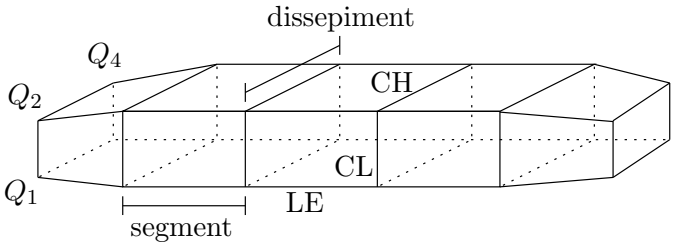

Figure 1: Sketch of a model with $N = 5$ segments and $d = 24$ corners. Dissepiments are introduced by compartmentalization of the body, see Sect. 2.2.

are included as part of the CLs and oblique muscles are neglected at present. See e.g. Fig. 1A in [32] for a schematic sketch of the muscle layers in the body wall of the leech. The shape of the model at time $t \in [0, T]$, $T > 0$ is determined by the coordinate vector $q(t) \in \mathbb{R}^{3d}$ of the corners with components $Q_i(t) \in \mathbb{R}^3$ for $i = 1 \dots d$. The velocities are given by $U_i(t) = \dot{Q}_i(t)$ with $u(t) = \dot{q}(t) \in \mathbb{R}^{3d}$ and we assume the total mass to be distributed over the whole body with lumped masses $m_i > 0$ in the corners.

2.1 The elastic edges

We assume that every elastic element acts as a combination of a spring and a dashpot arranged in parallel. This mechanical model (Voigt body) simulates the viscoelastic material of muscles, we refer to Sect. 2.11 in [12] for more details on the properties of this model like hysteresis, creep, and stress relaxation. In general, the length–tension relation of muscles is nonlinear, and in [38] the active and passive length–tension curves (LTCs) are fitted to experimental data of the activated and relaxed longitudinal muscle of the medicinal leech. However, as a first approximation we use Hooke's law combined with a linear damping term. Consider first a single elastic element between two adjacent corners $Q_i, Q_j \in \mathbb{R}^3$ with velocities $U_i, U_j \in \mathbb{R}^3$ for $i \neq j$ and $1 \leq i, j \leq d$. At time t the force exerted at Q_i by this elastic element is of the form

$$f_{ij}(t, q, u) = \Big(F_{ij}(Q_i, Q_j) - d_{ij} D_{ij}(Q_i, Q_j, U_i, U_j)\Big) n_{ij}, \quad n_{ij} = \frac{Q_j - Q_i}{\|Q_j - Q_i\|_2} \tag{1}$$

with the elastic and damping terms given by

$$F_{ij}(Q_i, Q_j) = a_{ij}(t) \left(\|Q_j - Q_i\|_2 - L_{ij}^{min}\right), \quad D_{ij}(Q_i, Q_j, U_i, U_j) = (U_i - U_j)^T n_{ij}. \tag{2}$$

For every single elastic element the minimum length L_{ij}^{min}, the damping parameter $d_{ij} \geq 0$, and the level of activation $a_{ij}(t) \in [0, 1]$ at time t are to be prescribed. So far only the elastic and damping properties in the direction n_{ij} of the muscles are

incorporated into the model, shear forces are not yet taken into account. Obviously, nonlinear length–tension relations of the muscles can be built into the model by an appropriate choice of the functions F_{ij}.

Depending on the position there are 3 or 4 elastic elements acting on each corner (see Fig. 1), so the total force acting on Q_i at time t results to

$$f_i(t,q,u) := \sum_{j\in I(i)} f_{ij}(t,q,u), \tag{3}$$

where the set $I(i) \subset \{1\dots d\}$ contains the indices of the corners adjacent to Q_i.

2.2 The constraint of constant volume

The model is based on the assumption that the total volume, which is the sum of the volumes of all segments, remains constant during the motion. In order to prevent volume exchanges, adjacent segments can also be grouped to compartments, so that in a model with m compartments we find the constraints

$$\sum_{j=\alpha_k}^{\beta_k} V_j(q(t)) = V_k^{tot}, \quad \text{for } k = 1\dots m. \tag{4}$$

Here V_k^{tot} is the given volume of the kth compartment, $V_j(q(t))$ expresses the volume of the jth segment in terms of the coordinate vector $q(t)$, and α_k and β_k denote the numbers of the first and the last segment in the kth compartment. In general, we also allow the volumes of the compartments to vary in time and finally find the constraints

$$g_k(t,q(t)) = 0, \;\; k = 1\dots m, \quad \text{where} \quad g_k(t,q) := \sum_{j=\alpha_k}^{\beta_k} V_j(q) - V_k^{tot}(t). \tag{5}$$

Notice that the given volume of the kth compartment is now time–dependent. The volume exchanges are assumed to be frictionless, therefore the constraints in (5) are holonomic. In [37] a formula for the volume $V_j(q) = V_j(Q_{4(j-1)+1},\dots,Q_{4(j-1)+8})$ of a single hexahedral segment $j \in \{1\dots N\}$ is derived using a trilinear transformation.

2.3 The equations of motion

The motion of the model is described by the coordinates and velocities of the corners, and the inner pressures in the compartments. Newton's second law together with d'Alembert's principle lead to Lagrange's equations of motion (see e.g. [13])

$$m_i\ddot{Q}_i(t) = f_i(t,q(t),u(t)) + \sum_{k=1}^{m} \nu_k(t)\frac{\partial g_k}{\partial Q_i}\Big(t,Q_1(t),\dots,Q_d(t)\Big), \quad i = 1\dots d \tag{6}$$

$$0 = g_k(t,q(t)), \quad k = 1\dots m \tag{7}$$

Here the total force acting on the corner Q_i is composed of the inner force (3) exerted by the elastic elements and the forces of constraint which arise from the volume constraints (5). The absolute value of the Lagrange multiplier $\nu_k(t)$ corresponds to the inner pressure in the kth compartment at time t (cf. Sect. 2 in [37]). Even though the model is geometrically simplified, the system contains $3d+3d+m = 549$ unknowns when a fully compartmentalized model ($m = N$) with $N = 21$ segments is used.

2.4 Collision with an obstacle

We consider the special case that the motion of the system of mass–points is constrained by an obstacle which is given by the hyperplane

$$\mathcal{H} := \{Q \in \mathbb{R}^3 : Q_1 = K\}, \;\; K > 0. \tag{8}$$

With the set $J := \{1, 4, 7, \ldots, 3d-2\} \subset I := \{1 \ldots 3d\}$ we find the unilateral constraints

$$q_j(t) - K \geq 0 \quad \text{for all } \; j \in J \tag{9}$$

and a constraint $j \in J$ is called "active" at time t if the corresponding mass–point $q_j(t)$ is in contact with the obstacle $\mathcal{H}$, i.e. $(q_j(t) - K) = 0$. We define the "active set" by

$$J_A(t) := \{j \in J : q_j(t) = K\}, \quad a(t) := \#J_A(t), \tag{10}$$

and the corresponding "passive set" $J_P(t) := J \backslash J_A(t)$ contains the indices of all "passive" constraints, i.e. $(q_j(t) - K) > 0$ for all $j \in J_P(t)$. Notice that every active constraint corresponds to a holonomic constraint of the form (7). With the settings

$$f(t,q,u) := \begin{pmatrix} f_1(t,q,u) \\ \vdots \\ f_d(t,q,u) \end{pmatrix}, \quad g(t,q) := \begin{pmatrix} g_1(t,q) \\ \vdots \\ g_m(t,q) \end{pmatrix}, \quad \nu := \begin{pmatrix} \nu_1 \\ \vdots \\ \nu_m \end{pmatrix},$$

and $G(t,q) := (\partial g/\partial q)(t,q) \in \mathbb{R}^{m,3d}$ we arrive at the DAE system

$$\dot{q}(t) = u(t) \tag{11}$$

$$M\dot{u}(t) = f(t, q(t), u(t)) + G(t, q(t))^T \nu(t) + H^T \lambda(t) \tag{12}$$

$$0 = g(t, q(t)) \tag{13}$$

with the complementarity conditions (Hertz–Signorini–Moreau 1963, see [29])

$$(q_j(t) - K) \geq 0, \quad \lambda_j(t) \geq 0, \quad (q_j(t) - K)\lambda_j(t) = 0 \quad \text{for all } \; j \in J, \tag{14}$$

see e.g. [9], [25], [30] for a general discussion. Here $H^T\lambda$ are the contact forces, where

$$\lambda = \left(\lambda_1, \lambda_4, \lambda_7, \ldots, \lambda_{3d-2}\right)^T \in \mathbb{R}^d, \quad H \in \mathbb{R}^{d,3d}, \; H_{ji} = \begin{cases} 1, & \text{if } i = 3j-2 \\ 0, & \text{otherwise} \end{cases}.$$

The vector $\nu \in \mathbb{R}^m$ in (12) contains the m Lagrange multipliers that correspond to the global holonomic constraints (13). The fact that the masses m_i might vary if considerable variations in the segmental volumes occur is not yet incorporated into the model. Therefore we find a constant diagonal mass–matrix

$$M := \operatorname{diag}(m_1, m_2, \ldots, m_{3d}) \in \mathbb{R}^{3d,3d} \tag{15}$$

that contains the lumped masses $m_{3i-2} = m_{3i-1} = m_{3i} > 0$ of the mass–points $i = 1 \ldots d$ as diagonal entries. In (12) the applied forces are given by $f(t,q,u)$ and the forces of constraint that maintain the global holonomic constraints (13) are given by $G(t,q)^T\nu$. The complementarity conditions (14) can be explained as follows: The frictionless contact of a single mass–point with the obstacle $\mathcal{H}$ is characterized by the three facts that the mass–point cannot penetrate the obstacle, the mass–point cannot pull on the obstacle, and either the mass-point presses on the obstacle or it is separated from the obstacle. The geometric condition of "no penetration" is given by the first inequality in (14), and the second inequality in (14) expresses the "no adhesion" condition. The equality condition of complementarity in (14) refers to the fact that at time t the mass–point is either distant and there is no contact force, i.e. $(q_j(t) - K) \neq 0$ and $\lambda_j(t) = 0$, or it is in contact with the obstacle and there is an interaction by a contact force, i.e. $(q_j(t) - K) = 0$ and $\lambda_j(t) \neq 0$. When the mass–point "touches" the obstacle, i.e. both $(q_j(t) - K)$ and $\lambda_j(t)$ are zero, we find a more complicated contact situation, see e.g. [2], [23], [30] for a detailed discussion. We will use $K = 0$ in the following, and we state a well–known result which will be used frequently (see e.g. [14] for a proof):

Lemma 2.1 *Let $M \in \mathbb{R}^{3d,3d}$ and $\mathcal{G} \in \mathbb{R}^{s,3d}$ be given such that rank$(\mathcal{G}) = s$ and M is positive definite. Then the block matrix*

$$N := \begin{pmatrix} M & \mathcal{G}^T \\ \mathcal{G} & 0 \end{pmatrix} \in \mathbb{R}^{3d+s,3d+s}$$

as well as its Schur complement $-\mathcal{G}M^{-1}\mathcal{G}^T \in \mathbb{R}^{s,s}$ is invertible.

2.5 Smooth motion

In time intervals where the active and passive sets are constant the equations of motion (11)-(13) together with the active constraints in (14) result to

$$\begin{aligned} \dot{q}(t) &= u(t) && (16)\\ M\dot{u}(t) &= f(t,q(t),u(t)) + G(t,q(t))^T\nu(t) + A(t)^T(A(t)H^T\lambda(t)) && (17)\\ 0 &= g(t,q(t)) && (18)\\ 0 &= A(t)q(t) && (19) \end{aligned}$$

$$A(t) \in \mathbb{R}^{a(t),3d},\ A_{ji}(t) = \begin{cases} 1, \text{ if } i = k_j \in J_A(t) = \{k_1,\ldots,k_{a(t)}\} \\ 0, \text{ otherwise} \end{cases}. \qquad (20)$$

The $a(t)$ active constraints are included as holonomic constraints with Lagrange multipliers $\Lambda(t) := A(t)H^T\lambda(t) \in \mathbb{R}^{a(t)}$, and (16)-(19) is a semi–explicit DAE system for (q,u,ν,Λ), see e.g. [3], [5], [9], [17]. The remaining components of $\lambda(t)$ are obtained from the complementarity conditions (14) as $\lambda_j(t) = 0$ for $j \notin J_A(t)$. Differentiating (18), (19) once and twice w.r.t. t yields the first and second order "hidden" constraints which are also fulfilled by a smooth solution of the system (16)-(19):

$$0 = g_t(t,q) + G(t,q)u,\ \ 0 = A(t)u, \quad \text{and} \qquad (21)$$

$$\begin{aligned} 0 &= \widetilde{g}(t,q,u) + G(t,q)M^{-1}\left[f(t,q,u) + G(t,q)^T\nu + A(t)^T(A(t)H^T\lambda(t))\right],\\ 0 &= A(t)M^{-1}\left[f(t,q,u) + G(t,q)^T\nu + A(t)^T(A(t)H^T\lambda(t))\right], \end{aligned} \qquad (22)$$

$$\text{where} \quad \widetilde{g}(t,q,u) := g_{tt}(t,q) + 2G_t(t,q)u + G_q(t,q)(u,u). \qquad (23)$$

For (t,q) fixed we have $g_{tt}(t,q) \in \mathbb{R}^m$, $G_t(t,q) \in \mathbb{R}^{3d,m}$, and $G_q(t,q) : \mathbb{R}^{3d} \times \mathbb{R}^{3d} \to \mathbb{R}^m$ is a bilinear mapping. We assume that the functions f and g have a sufficient number of continuous derivatives, and we set $\mathcal{V} := \mathbb{R}^{3d} \times \mathbb{R}^{3d} \times \mathbb{R}^m \times \mathbb{R}^d$. For $a < b$ and $s \geq 1$ we denote the left and right limits of a function $\psi \in \mathcal{C}((a,b),\mathbb{R}^s)$ at time $c \in (a,b)$ by $\psi^-(c)$ and $\psi^+(c)$, respectively. Furthermore, $J_A^-(c)$ and $J_A^+(c)$ denote the active sets before and after a collision or a lift–off. The corresponding passive sets are defined by $J_P^-(c) = J\backslash J_A^-(c)$ and $J_P^+(c) = J\backslash J_A^+(c)$.

2.6 The jump conditions

It turns out that the model (11)-(14) is not yet complete: The active and passive sets are time–dependent and can alter in the course of motion. In case of a collision a passive

constraint suddenly becomes active, and an active constraint becomes passive if the corresponding mass–point lifts off the obstacle. Events like this can cause discontinuities in the system and the equations of motion are no longer valid. Therefore jump conditions have to be derived that describe the behavior of the system if such an event occurs.
In order to approximate a rigid collision we use Newton's impact law, which relates the normal velocity $u_p^+(c)$ after the impact of a mass–point $p \in J_P^-(c)$ at time $c > 0$ to the normal velocity $u_p^-(c)$ before the impact:

$$q_p(c) = 0,\ u_p^-(c) < 0 \quad \Longrightarrow \quad u_p^+(c) = -\varepsilon u_p^-(c) \tag{24}$$

The constant $\varepsilon \in [0,1]$ is the coefficient of restitution. The value $\varepsilon = 1$ corresponds to the completely elastic case, and only for $\varepsilon = 0$ the collision is inelastic and we have $p \in J_A^+(c)$. The jump discontinuity in the normal velocity of the colliding mass–point, i.e. in the direction normal to the obstacle, is caused by an impulsive force (δ–distribution) which is applied at $t = c$, it approximates a large force with a short duration. At the time of impact there is not only an impulsive contact force $I^p = I^p(c) \in \mathbb{R}$ in the constraint $p \in J_P^-(c)$ that suddenly becomes active, we also have impulsive constraint forces $I^\lambda = I^\lambda(c) \in \mathbb{R}^{a^-(c)}$ and $I^\nu = I^\nu(c) \in \mathbb{R}^m$ caused by the constraints in $J_A^-(c)$ that are already active as well as the global holonomic constraints (13). These impulses lead to jump discontinuities in the velocities of all mass–points in the system, and by local conservation of impulses we find the jump condition

$$M\Big(u^+(c) - u^-(c)\Big) = G(c,q(c))^T I^\nu + A^-(c)^T I^\lambda + e_p I^p, \tag{25}$$

where $e_p \in \mathbb{R}^{3d}$ is the pth unit vector. This equation is used at $t = c$ instead of the equations of motion (11)-(14), for a derivation of (25) see e.g. [15]. In [2] it is shown that (12) is still valid at $t = c$ in the sense of distributions if (25) holds.
Additional conditions are derived by the fact that the first order hidden constraints (21) have to be fulfilled after the impact, i.e. consistent initial values are needed. For the global holonomic constraints (13) and the constraints in $J_A^-(c)$ that are already active, equations (21) leads to

$$g_t(c,q(c)) + G(c,q(c))u^+(c) = 0, \quad A^-(c)u^+(c) = 0. \tag{26}$$

Obviously, there might be a whole subset of indices in $J_P^-(c)$ such that all mass–points with indices in this subset collide with the obstacle at the same time. Newton's impact law (24) for inelastic collisions ($\varepsilon = 0$), the condition for the impulses (25), and the

conditions for the first order hidden constraints (26) lead to the system

$$\begin{pmatrix} M & G(c,q(c))^T & A^+(c)^T \\ G(c,q(c)) & 0 & 0 \\ A^+(c) & 0 & 0 \end{pmatrix} \begin{pmatrix} u^+(c) \\ -I^\nu \\ -I_C^\lambda \end{pmatrix} = \begin{pmatrix} Mu^-(c) \\ -g_t(c,q(c)) \\ 0 \end{pmatrix} \tag{27}$$

with the impulses $I_C^\lambda = I_C^\lambda(c) \in \mathbb{R}^{a^+(c)}$. If the rank condition

$$\operatorname{rank} \begin{pmatrix} G(t,q) \\ H \end{pmatrix} = m + d \tag{28}$$

is fulfilled at $(t,q) = (c,q(c))$, Lemma 2.1 implies that (27) can be solved uniquely for $u^+(c)$, I^ν, and I_C^λ. After the collision the Lagrange multipliers are determined uniquely by the second order hidden constraints (22) with the new active set $J_A^+(c)$. These also involve $u^+(c)$ and $A^+(c)$, and therefore we also find jump discontinuities in the Lagrange multipliers, see [2] for details.

During a lift–off the solution $(q,u,\nu,\lambda) \in \mathcal{V}$ is continuous, but discontinuities in $\dot\nu$ and $\dot\lambda$ are possible. Usually, the contact force λ_p of an active constraint $p \in J_A^-(c)$ becomes zero at $t = c$ with $\dot\lambda_p^-(c) < 0$ and the corresponding mass–point lifts off the obstacle. Because of the complementarity conditions (14) the contact force has to be zero after the lift–off, so there is a jump discontinuity in $\dot\lambda_p$ and this also affects $\dot\nu$ and $\dot\lambda_j$ for $j \in J_A^+(c) = J_A^-(c)\backslash\{p\}$ (details can be found in [2]):

$$\begin{pmatrix} \dot\nu^+(c) - \dot\nu^-(c) \\ A^+(c)H^T(\dot\lambda^+(c) - \dot\lambda^-(c)) \end{pmatrix} = D(c,q(c))^{-1} \begin{pmatrix} -G(c,q(c))M^{-1}e_p\dot\lambda_p^-(c) \\ -A^+(c)M^{-1}e_p\dot\lambda_p^-(c) \end{pmatrix},$$

$$\text{where} \quad D(t,q(t)) := \begin{pmatrix} G(t,q) \\ A(t) \end{pmatrix} M^{-1} \begin{pmatrix} G(t,q) \\ A(t) \end{pmatrix}^T. \tag{29}$$

2.7 Contact with tangential friction

An active constraint $j \in J_A$ prevents the corresponding mass–point from penetrating the obstacle, this is done by a constraint force $\lambda_j \geq 0$ that acts in direction normal to the obstacle. However, the mass–point might slide on the obstacle in tangential direction and we have to model the friction forces which depend on the material of the obstacle, the roughness of the surface, and the normal contact force.

We assume that there is no grease or fluid between the sliding mass–points and the obstacle and therefore we use a model of dry friction. Coulomb's friction law states that during sliding the tangential friction force is proportional to the normal contact

force, the relative tangential velocity, and the coefficient $\mu > 0$ of sliding friction (see e.g. [9], [15], [26], [30]). The friction force acts in direction opposite to the tangential velocity, and when the tangential velocity becomes zero the mass–point starts to stick on the obstacle. During sticking (or lock–up) the tangential friction force is bounded by the coefficient $\mu_0 > 0$ of static friction times the normal contact force λ_j, and the mass–point starts to slide again if this bound is violated.

We introduce a new set which contains the indices of all active constraints that correspond to mass–points that stick on the obstacle:

$$J_S(t) := \{j \in J_A(t) \mid u_j^t(t) = 0\}, \quad s(t) := \#J_S(t),$$

where $u_j^t := (u_{j+1}^2 + u_{j+2}^2)^{1/2}$ is the relative tangential velocity. The friction forces in y– and z–direction on the hyperplane $\mathcal{H}$ defined in (8) are denoted by r_{j+1} and r_{j+2}, respectively. For $j \in J_P$ there is no friction force and we set $r_{j+1} = r_{j+2} = 0$. In case $j \in J_A$ we have

$$\text{sticking, } u_j^t = 0 \implies \sqrt{r_{j+1}^2 + r_{j+2}^2} \le \mu_j^0 \lambda_j, \quad j \in J_S \tag{30}$$

$$\text{sliding, } u_j^t \neq 0 \implies \begin{pmatrix} r_{j+1} \\ r_{j+2} \end{pmatrix} = -\frac{1}{u_j^t} \begin{pmatrix} u_{j+1} \\ u_{j+2} \end{pmatrix} \mu_j(u_j^t)\lambda_j, \quad j \notin J_S \tag{31}$$

where $(r_{j+1}^2 + r_{j+2}^2)^{1/2}$ is the absolute value of the tangential friction force during sticking. During sliding the friction forces are defined by (31) and have to be added to the right hand side of (12). The coefficient $\mu : \mathbb{R} \to \mathbb{R}_+$ of sliding friction usually depends on the relative tangential velocity. In most applications Stribeck curves which coincide with the coefficient μ^0 of static friction at zero velocity are used, see Figure 2. During sticking they are given by Lagrange multipliers that correspond to constraints that fix the actual position and prevent tangential movement. This will be described in detail in Sect. 3.4 when we present the numerical methods.
During a sliding/sticking transition the solution $(q, u, \nu, \lambda) \in \mathcal{V}$ of (11)-(14) is continuous, but jump discontinuities in the accelerations and the friction forces r_{j+1}, r_{j+2} for $j \in J_S$ might occur: If a sliding mass–point starts to stick we find jump discontinuities in the friction forces and therefore also in the accelerations (see also the numerical experiments in Sect. 2.4, Fig. 4D).

Notice that the sticking/sliding condition for a constraint $j \in J_A$ is given by the relative tangential velocity u_j^t and not by the velocities u_{j+1} and u_{j+2} in y– and z–direction.

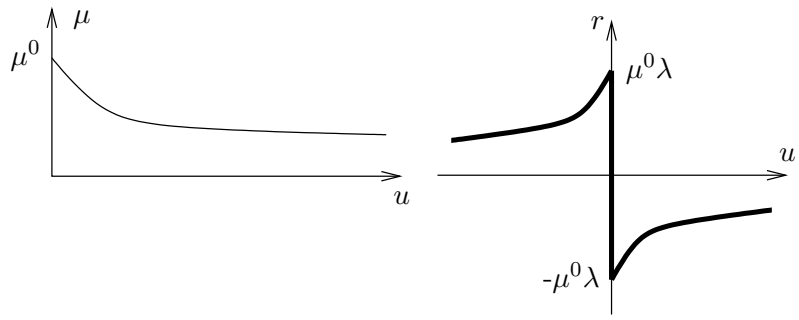

Figure 2: Stribeck curve μ with $\mu(0) = \mu^0$ (left) and corresponding friction force r (right).

Therefore Coulomb's friction law cannot be incorporated into the system (11)-(14) by simple complementarity conditions as in the case of the collision/lift–off conditions. In the numerical methods (see Sect. 3) we assume $u_{j+1} \equiv 0$ for all $j \in J_A$ and include only the friction forces in z–direction (one–dimensional case). This simplifies the conditions in (30),(31) considerably since the relative tangential velocity u_j^t is replaced by $|u_{j+2}|$. See [23] and [30] for a discussion of several two–dimensional friction models and Stribeck curves with hysteresis effects ($\mu^0 > \mu(0)$).

3 Numerical methods

In this chapter we describe the numerical methods that are used to solve the equations of motion (11)-(14) with global holonomic and unilateral constraints. In time intervals where no collision or lift–off occurs the DAE (16)-(19) with the current active set is solved by standard numerical methods implemented in the code MEXAX, see [28]. In case of a collision or a lift–off the integration of the DAE is interrupted, the active and passive sets are modified, and new initial values are determined by the jump conditions (27) in case of an impact. Similarly, in the presence of tangential friction forces the integration is interrupted when a sticking/sliding transition occurs, and the stiction set has to be modified. We present a switching algorithm which controls the event localization during the integration and the modification of the active/passive/stiction sets.

3.1 Discretization of the equations of motion

We start by describing the basic discretization method which is used to solve the DAE system (16)-(19) with the current active set in time intervals where no collision or lift–off occurs. We consider first the frictionless case, the incorporation of the friction forces

will be described later on in Sect. 3.4.

In the code MEXAX a modified half–explicit Euler method is used which is explicit in the differential part and implicit in the algebraic part of the DAE. Applying the standard half–explicit Euler method directly to the system (16)-(19) leads to a large nonlinear system which has to be solved in every time step, see e.g. [27]. This is avoided if we replace (18),(19) by the first order hidden constraints, and we find the system

$$\begin{aligned} \dot{q} &= u && (32)\\ M\dot{u} &= f(t,q,u) + G(t,q)^T\nu + A(t)^T\left(A(t)H^T\lambda\right) && (33)\\ 0 &= g_t(t,q) + G(t,q)u && (34)\\ 0 &= A(t)u && (35) \end{aligned}$$

for $t \in [0,T]$, where $\lambda_j(t) = 0$ for $j \in J_P(t)$ by the complementarity conditions (14). Using the fixed step size $h = (T/N) > 0$ with $N \in \mathbb{N}$ we are looking for an approximation $(q^{n+1}, u^{n+1}, \nu^{n+1}, \lambda^{n+1}) \in \mathcal{V}$ at $t^n = nh \in [0,T]$ for $n = 0 \ldots N$. Given consistent initial values (q^0, u^0) the standard half–explicit Euler method for the above system yields

$$\begin{aligned} q^{n+1} &= q^n + hu^n && (36)\\ Mu^{n+1} &= Mu^n + hf(t^n,q^n,u^n) + hG(t^n,q^n)^T\nu^{n+1} + hA(t^n)^T\left(A(t^n)H^T\lambda^{n+1}\right) && (37)\\ 0 &= g_t(t^{n+1},q^{n+1}) + G(t^{n+1},q^{n+1})u^{n+1} && (38)\\ 0 &= A(t^{n+1})u^{n+1} && (39) \end{aligned}$$

for $n = 0 \ldots N-1$. The special structure of the system allows to calculate the position vector q^{n+1} directly from (36). Notice that $A(t^n) = A(t^{n+1})$ since we only consider time intervals where the active set is constant. Replacing $G(t^n,q^n)$ by $G(t^{n+1},q^{n+1})$ in (37) leads to the linear system

$$\Gamma(t^{n+1},q^{n+1}) \begin{pmatrix} u^{n+1} \\ -h\nu^{n+1} \\ -hA(t^{n+1})H^T\lambda^{n+1} \end{pmatrix} = \begin{pmatrix} Mu^n + hf(t^n,q^n,u^n) \\ -g_t(t^{n+1},q^{n+1}) \\ 0 \end{pmatrix} \qquad (40)$$

$$\text{where} \quad \Gamma(t,q) := \begin{pmatrix} M & G(t,q)^T & A(t)^T \\ G(t,q) & 0 & 0 \\ A(t) & 0 & 0 \end{pmatrix} \qquad (41)$$

Together with $\lambda_j^{n+1} = 0$ for $j \in J_P(t^{n+1})$ this system has a unique solution $(u^{n+1}, \nu^{n+1}, \lambda^{n+1})$ by Lemma 2.1 if the rank condition (28) holds.

3.2 Projections and jump conditions

An analytical solution of the system (32)-(35) on velocity level also fulfills the original constraints (18),(19) on position level if the initial values are consistent, but this is in general not true for an approximate solution of (36)-(39). To enforce the original constraints after each times step, q^{n+1} is projected orthogonally onto the position manifold defined by (18),(19) for $t = t^{n+1}$, i.e. we look for a $\widetilde{q}^{n+1}$ such that $||q^{n+1} - \widetilde{q}^{n+1}||_M$ is minimized. This leads to a nonlinear system which is solved by a simplified Newton method with iteration matrix $\Gamma(t^{n+1}, q^{n+1})$ defined in (41). Next, we have to adapt the velocity vector u^{n+1} to the projected position vector $\widetilde{q}^{n+1}$ by an orthogonal projection onto the velocity manifold defined by (21), where $t = t^{n+1}$ and $q = \widetilde{q}^{n+1}$. As above we choose $\widetilde{u}^{n+1}$ such that $||u^{n+1} - \widetilde{u}^{n+1}||_M$ is minimized. In contrast to the projection onto the position manifold this leads to the linear system

$$\Gamma(t^{n+1}, \widetilde{q}^{n+1}) \begin{pmatrix} \widetilde{u}^{n+1} \\ b_1 \\ b_2 \end{pmatrix} = \begin{pmatrix} Mu^{n+1} \\ -g_t(t^{n+1}, \widetilde{q}^{n+1}) \\ 0 \end{pmatrix} \tag{42}$$

with Γ defined in (41) and vectors $b_1 \in \mathbb{R}^m$ and $b_2 \in \mathbb{R}^{a(t^{n+1})}$. We refer to [2], [11], [28] for details.

The above projection methods are used in intervals where the active set is constant. If a collision of a mass–point with the obstacle occurs at $t^{n+1} \in [0, T]$ the active set is modified and the matrix $A^-(t^{n+1})$ is replaced by $A^+(t^{n+1})$. Furthermore, new initial values for the velocities have to be determined and the jump conditions (27) read

$$\begin{pmatrix} M & G(t^{n+1}, q^{n+1})^T & A^+(t^{n+1})^T \\ G(t^{n+1}, q^{n+1}) & 0 & 0 \\ A^+(t^{n+1}) & 0 & 0 \end{pmatrix} \begin{pmatrix} u^* \\ -I^\nu \\ -I_C^\lambda \end{pmatrix} = \begin{pmatrix} Mu^{n+1} \\ -g_t(t^{n+1}, q^{n+1}) \\ 0 \end{pmatrix} \tag{43}$$

with the impulses $I^\nu \in \mathbb{R}^m$ and $I_C^\lambda \in \mathbb{R}^{a^+(t^{n+1})}$, the position vector q^{n+1}, and the velocity vectors u^{n+1} and u^* before and after the impact, respectively. New initial values for the Lagrange multipliers after the collision are not needed in the half–explicit discretization method presented in Sect. 3.1. They are calculated by (40) in the next step after the collision using the new initial values for the position and velocity vectors.

Notice that (43) coincides with (42). This is no surprise since after an inelastic impact among all admissible velocities in the velocity manifold the nearest one is chosen and

this is simply the orthogonal projection. In MEXAX various linear algebra options are included and we decided to use the sparse direct matrix solver MA28 from the Harwell Sparse Matrix Library (NAG Ltd.). Notice that all linear systems that arise in the discretization procedure, the projection steps, and the jump conditions have the same block diagonal structure.

3.3 Extrapolation, dense output, and event localization

To improve the accuracy of the numerical solution adaptive extrapolation methods with order and step size control are used in MEXAX, a detailed description can be found in [11].

While extrapolation methods are important to improve the accuracy of the numerical solution, the combined order and step size control usually leads to large step sizes during the integration. For the purpose of a graphical representation as well as for event localization problems the solution has to be determined at prescribed points. Decreasing the step size would increase the computational cost and interfere with the combined order and step size control. Therefore a suitable dense output method has to be used which yields a functional description of the numerical solution rather than approximations at discrete points. See [11], [16], [19], [28] for a detailed description of the method and the implementation in MEXAX, the basic idea is as follows: In addition to the numerical solution at the endpoints of the time interval $[t^n, t^n + H]$, approximations of the solution derivatives are computed by divided forward and backward differences. Again, these approximations can be improved by extrapolation methods as above. Finally, Hermite–interpolation (see e.g. Sect. 2.1.5 in [34]) yields a polynomial which coincides with the numerical solution and the approximations of the solution derivatives at t^n and $t^n + H$. The error of the polynomial approximation is of the same order as the global error of the numerical method provided that sufficiently many approximate solution derivatives with a high accuracy are used to generate the polynomial.

The dense output method is used to localize zeroes of switching functions between two integration points t^n and $t^n + H$, i.e. the nonlinear root–finding problem

$$\Phi(t) = 0 \quad \text{with} \quad \Phi : [t^n, t^n + H] \to \mathbb{R}$$

has to be solved. The occurrence of a root is indicated by a sign change

$$\Phi(t^n)\Phi(t^n + H) < 0, \tag{44}$$

and the first (leftmost) root is computed by a modified Newton method. It is included as integration point t^{n+1}. To avoid problems with switching functions that are zero for a certain period of time the conditions

$$|\Phi(t^n)| \geq \overline{\Phi}, \quad |\Phi(t^n + H)| \geq \overline{\Phi}$$

with a given residual $\overline{\Phi} > 0$ are used in addition to (44). Switching functions with an even number of zeroes or a zero with an even multiplicity in the time interval $[t^n, t^n + H]$ can be handled by performing additional sign checks similar to (44) in certain subintervals of $[t^n, t^n + H]$. We refer to [28] for further details.

3.4 Friction forces

For all active constraints $j \in J_A(t^{n+1})$ we have to add tangential friction forces to the system, see Sect. 2.7. We consider only the one–dimensional case and assume $u_{j+1}^{n+1} = 0$, this simplifies the sticking/sliding conditions in (30) and (31), see Sect. 2.7. For every element of the stiction set

$$J_S(t^{n+1}) = \{j \in J_A(t^{n+1}) \mid u_{j+2}^{n+1} = 0\} \quad \text{with} \quad s(t^{n+1}) = \#J_S(t^{n+1})$$

we have to add a constraint that fixes the actual position q_{j+2}^{n+1}. The corresponding Lagrange multiplier r_{j+2}^{n+1} is bounded by the coefficient of static friction μ_j^0 times the contact force λ_j^{n+1}, i.e.

$$|r_{j+2}^{n+1}| \leq \mu_j^0 \lambda_j^{n+1},$$

see (30). During sliding the tangential velocity u_{j+2}^{n+1} is nonzero, we have $j \notin J_S(t^{n+1})$ and the external force

$$r_{j+2}^{n+1} = \begin{cases} -\mu_j^{n+1}\lambda_j^{n+1}, & \text{if } u_{j+2}^{n+1} > 0 \\ \mu_j^{n+1}\lambda_j^{n+1}, & \text{if } u_{j+2}^{n+1} < 0 \end{cases} \quad \text{with } \mu_j^{n+1} := \mu_j(|u_{j+2}^{n+1}|) \tag{45}$$

acting in opposite sliding direction is added, see (31). In time intervals where the active, passive, and stiction sets are constant the linear system (40) therefore extends to

$$\begin{pmatrix} M & G(t^{n+1},q^{n+1})^T & A(t^{n+1})^T & S(t^{n+1})^T \\ G(t^{n+1},q^{n+1}) & 0 & 0 & 0 \\ A(t^{n+1}) & 0 & 0 & 0 \\ S(t^{n+1}) & 0 & 0 & 0 \end{pmatrix} \begin{pmatrix} u^{n+1} \\ -h\nu^{n+1} \\ -hA(t^{n+1})H^T\lambda^{n+1} \\ -hS(t^{n+1})H^T r^{n+1} \end{pmatrix}$$
$$= \begin{pmatrix} Mu^n + hf(t^n,q^n,u^n) + hR(t^n)^T R(t^n)H^T r^n \\ -g_t(t^{n+1},q^{n+1}) \\ 0 \\ 0 \end{pmatrix} \tag{46}$$

$$S(t) \in \mathbb{R}^{s(t),3d},\ S_{ji}(t) := \begin{cases} 1, \text{ if } i = k_j \in J_S(t) = \{k_1,\ldots,k_{s(t)}\} \\ 0, \text{ otherwise} \end{cases}, \quad r^n := \begin{pmatrix} r_3^n \\ r_6^n \\ \vdots \\ r_{3d}^n \end{pmatrix}$$

$$R(t) \in \mathbb{R}^{a(t)-s(t),3d},\ R_{ji}(t) := \begin{cases} 1, \text{ if } i = k_j \in J_A(t)\backslash J_S(t) = \{k_1,\ldots,k_{a(t)-s(t)}\} \\ 0, \text{ otherwise} \end{cases}.$$

In addition, we set $\lambda_j^{n+1} = r_{j+2}^{n+1} = 0$ for all $j \in J_P(t^{n+1})$. The projection methods as well as the jump conditions in Sect. 3.2 are extended analogously and linear systems with block matrices similar to that in the above system (46) have to be solved. The rank condition (28) holds for $(t,q) = (t^{n+1},q^{n+1})$ since $G(t^{n+1},q^{n+1})$, $A(t^{n+1})$, and $S(t^{n+1})$ have linear independent row vectors, and therefore the matrix is invertible by Lemma 2.1. Notice that the forces r_{j+2}^n of sliding friction that occur on the right hand side of (46) for $j \in J_A(t^n)\backslash J_S(t^n)$ involve the Lagrange multipliers λ_j^n. Since we do not explicitly determine the values of λ_j^n after a collision at t^n by the second order hidden constraints we simply keep the values of r_{j+2}^n from the previous step. This is reasonable for small coefficients μ_j^n of sliding friction.

Remark 3.1

The external forces of sliding friction defined in (45) involve the Lagrange multipliers, therefore existence and uniqueness of a solution of the DAE system (16)-(19) with friction

forces introduced as above can only be guaranteed if the matrix

$$\begin{pmatrix} M & G(t,q)^T & (A(t)+R^\mu(t))^T & S(t)^T \\ G(t,q) & 0 & 0 & 0 \\ A(t) & 0 & 0 & 0 \\ S(t) & 0 & 0 & 0 \end{pmatrix} \text{ is invertible, where}$$

$$R^\mu(t) \in \mathbb{R}^{a(t)-s(t),3d},\ R^\mu_{ji}(t) = \begin{cases} -\mu_j(t), \text{ if } i = k_j \in J_A(t)\backslash J_S(t), \text{ and } u_{j+2}(t) > 0 \\ \mu_j(t), \text{ if } i = k_j \in J_A(t)\backslash J_S(t), \text{ and } u_{j+2}(t) < 0 \\ 0, \text{ otherwise} \end{cases}.$$

The nonsingularity of this matrix is needed to uniquely determine the Lagrange multipliers from the 2nd order hidden constraints (see also Lemma 2.1). However, if the coefficients $\mu_j(t)$ of sliding friction are small enough it can be shown by a perturbation Lemma (see e.g. [31]) that the above matrix is still invertible if the rank condition (28) holds. In [11], [28] a modified discretization method is proposed for applications with large coefficients of sliding friction.

3.5 The switching algorithm

The techniques presented in the previous sections are now combined to an algorithm that controls the event localization and the modifications of the active/passive/stiction sets during the integration, see Fig. 3. The basic idea is to use the discretization method described in Sect. 3.1 and 3.4 for the integration of the DAE in time intervals where the active set is constant. During the integration switching functions

$$\phi_j(t^{n+1}, q^{n+1}, u^{n+1}, \lambda^{n+1}, r^{n+1}) = \begin{cases} q_j^{n+1}, \text{ if } j \in J_P(t^{n+1}) \\ \lambda_j^{n+1}, \text{ if } j \in J_A(t^{n+1}) \\ u_{j+2}^{n+1}, \text{ if } j \in J_A(t^{n+1})\backslash J_S(t^{n+1}) \\ |r_{j+2}^{n+1}| - \mu_j^0 \lambda_j^{n+1}, \text{ if } j \in J_S(t^{n+1}) \end{cases}$$

for all $j \in J$ indicate events like collision, lift–off, or sticking/sliding transition. Between two integration steps the arguments of ϕ_j are taken from the values of the interpolation polynomial generated by the dense output method, see Sect. 3.3. In addition, these values are projected onto the position– and the velocity manifold as described in Sect. 3.2. If a root for one of the switching functions is found, the integration is interrupted, the sets are modified, and new initial values are calculated by the jump conditions (43) in case of a collision. Then the integration is continued until another event occurs or the end of the time interval $[0, T]$ is reached. During the integration a variable step size

is used (see Sect. 3.5). In addition, the dense output method yields a solution output for a given equidistant grid with step size $\widetilde{h} > 0$. However, the roots of the switching functions are not known a priori, so if a root is found at an integration point t^{n+1} the next step of the dense output method is performed with size $\widetilde{h} - (t^{n+1} - t^n)$.

After a collision of one or more mass–points at t^{n+1} we might find a negative Lagrange multiplier which corresponds to an active constraint. Furthermore, in the case of a lift–off as well as a transition from sticking to sliding we might find inconsistencies in the active/passive/sticking sets. For these problems the solution of an LCP is proposed in [2] and [30] to determine consistent sets that remain constant at least in infinitesimal time. However, it turns out that in the simulations such incompatibilities seldom occur. Therefore we do not solve an LCP and simply check if $\lambda_j^{n+2} > 0$ for all $j \in J_A(t^{n+2})$ and $|r_{j+2}^{n+2}| < \mu_j^0 \lambda_j^{n+2}$ for all $j \in J_S(t^{n+2})$ in the next step t^{n+2} after such an event. The integration is aborted if an inconsistency occurs, see Fig. 3 for an overview of the algorithm.

4 Numerical results

We simulate the collision of the non–compartmentalized model in the maximally shortened state (LEs maximally activated and CEs at rest) with the obstacle $\mathcal{H}$, see Fig. 4. The coefficients of static and sliding friction are set to constant and equal values for all corners ($\mu = 0$ and $\mu = 0.3$) and the simulation is started with initial velocity $U_i(0) = (-10, 0, -10)^T$ for $i = 1 \dots d$. At $t \approx 0.24$ the corners $Q_1 \dots Q_4$ collide with $\mathcal{H}$ and in the frictionless case ($\mu = 0$) the model starts to slide until all 4 corners lift off simultaneously at $t \approx 0.5$ (see Fig. 4, diagram A and left picture). In the presence of tangential friction ($\mu = 0.3$) the 4 corners start to stick on the obstacle at $t \approx 0.36$. The whole body bends, Q_2 and Q_4 lift off at $t \approx 0.375$, and Q_1 and Q_3 finally lift off at $t \approx 0.4$ (see diagram A and right picture in Fig. 4). The jump discontinuities in the internal pressure $|\nu|$, the contact force λ_2, and the (horizontal) x–velocity U_{21} of the corner Q_2 at the time $t \approx 0.24$ of impact are shown in Fig. 4B&C. Furthermore, Fig. 4D shows the friction force acting on Q_2 in case $\mu = 0.3$: When the (vertical) z–velocity U_{23} becomes zero the corner Q_2 starts to stick on the obstacle and we find forces of static friction, i.e. constraint forces that fix the actual z–position Q_{23}. Notice that the friction force acting on Q_2 shows jump discontinuities when a transition from sliding to sticking occurs at $t \approx 0.36$ and when Q_2 lifts off during sticking at $t \approx 0.375$.

References

[1] Alscher, C. & Beyn, W.–J.: Simulating the motion of the leech: A biomechanical application of DAEs. *Numerical Algorithms* 19, 1-12, 1998.

[2] Alscher, C.: Equations of constrained motion: Perturbation analysis and application to the hydrostatic skeleton. Ph.D. thesis, University of Bielefeld, appeared as: Fortschritt–Berichte VDI, Reihe 20, Nr. 307, Düsseldorf, 2000.

[3] Arnold, M.: Zur Theorie und zur numerischen Lösung von Anfangswertproblemen für differentiell–algebraische Systeme von höherem Index. Fortschritt–Berichte VDI, Reihe 20, Nr. 264, Düsseldorf, 1998.

[4] Beyn, W.–J. & Wadepuhl, M.: Verzeigung in einem Finite–Elemente Modell für das hydrostatische Skelett. *Z. angew. Math. Mech.* 70, T272-T274, 1990.

[5] Brenan, K.E., Campbell, S.L. & Petzold, L.R.: Numerical solution of initial–value problems in differential–algebraic equations. SIAM, Philadelphia, 1996.

[6] Chapman, G.: On the movement of worms. *J. exp. Biol.* 27, 29-39, 1950.

[7] Chiel, H.J., Crago, P., Mansour, J.M. & Hathi, K.: Biomechanics of a muscular hydrostat: A model of lapping by a reptilian tongue. *Biol. Cybern.* 67, 403-415, 1992.

[8] Cottle, R.W., Pang, J.–S., & Stone, R.E.: The linear complementarity problem. Academic Press, San Diego, 1992.

[9] Eich-Soellner, E. & Führer, C.: Numerical methods in multibody dynamics. B.G. Teubner, Stuttgart, 1998.

[10] Ekeberg, Ö.: A combined neuronal and mechanical model of fish swimming. *Biol. Cybern.* 69, 1-12, 1993.

[11] Engstler, C.: Numerische Lösung differentiell–algebraischer Gleichungen der Mehrkörperdynamik durch Extrapolationsverfahren. Diplomarbeit, Universität Innsbruck, 1993.

[12] Fung, Y.C.: Biomechanics: Mechanical properties of living tissues (2nd edition). Springer, New York, 1993.

[13] Greenwood, D.T.: Classical Dynamics. Prentice-Hall, Englewood Cliffs, N.J, 1977.

[14] Haug, E.J.: Computer aided kinematics and dynamics of mechanical systems. Volume I: Basic methods. Allyn and Bacon, Boston, 1983.

[15] Haug, E.J., Wu, S.C. & Yang, S.M.: Dynamics of mechanical systems with Coulomb friction, stiction, impact and constraint addition–deletion — I. Theory. *Mechanism and Machine Theory* 21, No. 5, 401-406, 1986.

[16] Hairer, E., Nørsett, S.P. & Wanner, G.: Solving ordinary differential equations — I. Nonstiff problems. Springer–Verlag, 1987.

[17] Hairer, E., Lubich, Ch. & Roche, M.: The numerical solution of differential–algebraic systems by Runge–Kutta methods. *Lecture Notes in Mathematics*, Springer–Verlag, 1989.

[18] Hairer, E., Nørsett, S.P. & Wanner, G.: Solving ordinary differential equations — II. Stiff and differential–algebraic problems. Springer–Verlag, 1991.

[19] Hairer, E. & Ostermann, A.: Dense output for extrapolation methods. *Numer. Math.* 58, 419-439, 1990.

[20] Jordan, C.E.: Mechanics and dynamics of swimming in the medicinal leech Hirudo medicinalis. Ph.D. thesis, University of Washington, 1994.

[21] Kier, W.M. & Smith, K.K.: Tongues, tentacles and trunks: the biomechanics of movement in muscular hydrostats. *Zool. J. Linn. Soc.* 83, 307-324, 1985.

[22] Kilmister, C.W. & Reeve, J.E.: Rational mechanics. Longmans, London, 1966.

[23] Klisch, T.: Kontaktmechanik in Starrkörpersystemen. Dissertation, TU München, Shaker Verlag, Aachen, 1997.

[24] Kristan, W.B. & Stent, G.S. & Ort, C.A.: Neuronal control of swimming in the medicinal leech (dynamics of the swimming rhythm). *J. Comp. Physiol.* 97-119, 1974.

[25] Lötstedt, P.: Mechanical systems of rigid bodies subject to unilateral constraints. *SIAM J. Appl. Math.* 42, No. 2, 281-296, 1982.

[26] Lötstedt, P.: Numerical simulation of time–dependent contact and friction problems in rigid body mechanics. *SIAM J. Sci. Stat. Comp.* 5, No. 2, 370-393, 1984.

[27] Lubich, Ch.: Extrapolation integrators for constrained multibody systems. *IMPACT Comp. Sci. Eng.* 3, 213-234, 1991.

[28] Lubich, Ch., Nowak, U., Pöhle, U. & Engstler, C.: MEXX–Numerical software for the integration of constrained mechanical multibody systems. Preprint SC 92-12, Konrad–Zuse–Zentrum für Informationstechnik, Berlin, 1992.

[29] Moreau, J.J.: Les liaisons unilatérales et le Principe de Gauss. *C.R. Acad. Sci., Paris* 256, 871-874, 1963.

[30] Pfeiffer, F. & Glocker, Ch.: Multibody dynamics with unilateral contacts. John Wiley & Sons, 1996.

[31] Schwetlick, H.: Numerische Lösung nichtlinearer Gleichungen. R. Oldenbourg Verlag, 1979.

[32] Skierczynski, B.A., Wilson, R.J.A., Kristan, W.B. & Skalak, R.: A model of the hydrostatic skeleton of the leech. *J. theor. Biol.* 181, 329-342, 1996.

[33] Stern–Tomlinson, W., Nusbaum, M.P., Perez, L.E. & Kristan, W.B.: A kinematic study of crawling behavior in the leech, Hirudo medicinalis. *J. Comp. Physiol. A* 158, 593-603, 1986.

[34] Stoer, J.: Numerische Mathematik I (6. Auflage). Springer–Verlag, 1993.

[35] Van Leeuwen, J.L. & Kier, W.M.: Functional design of tentacles in squid: linking sacomere ultrastructure to gross morphological dynamics. *Phil. Trans. R. Soc. Lond. B* 352, 551-571, 1997.

[36] Van Leeuwen, J.L.: Why the chameleon has spiral–shaped muscle fibres in its tongue. *Phil. Trans. R. Soc. Lond. B* 352, 573-589, 1997.

[37] Wadepuhl, M. & Beyn, W.–J.: Computer simulation of the hydrostatic skeleton. The physical equivalent, mathematics and application to worm–like forms. *J. theor. Biol.* 136, 379-402, 1989.

[38] Wadepuhl, M., Beyn, W.–J., & Alscher, C.: Stepwise adaptation of a computer model to the leech Hirudo medicinalis L. Preprint, FSPM, University of Bielefeld, 2000.

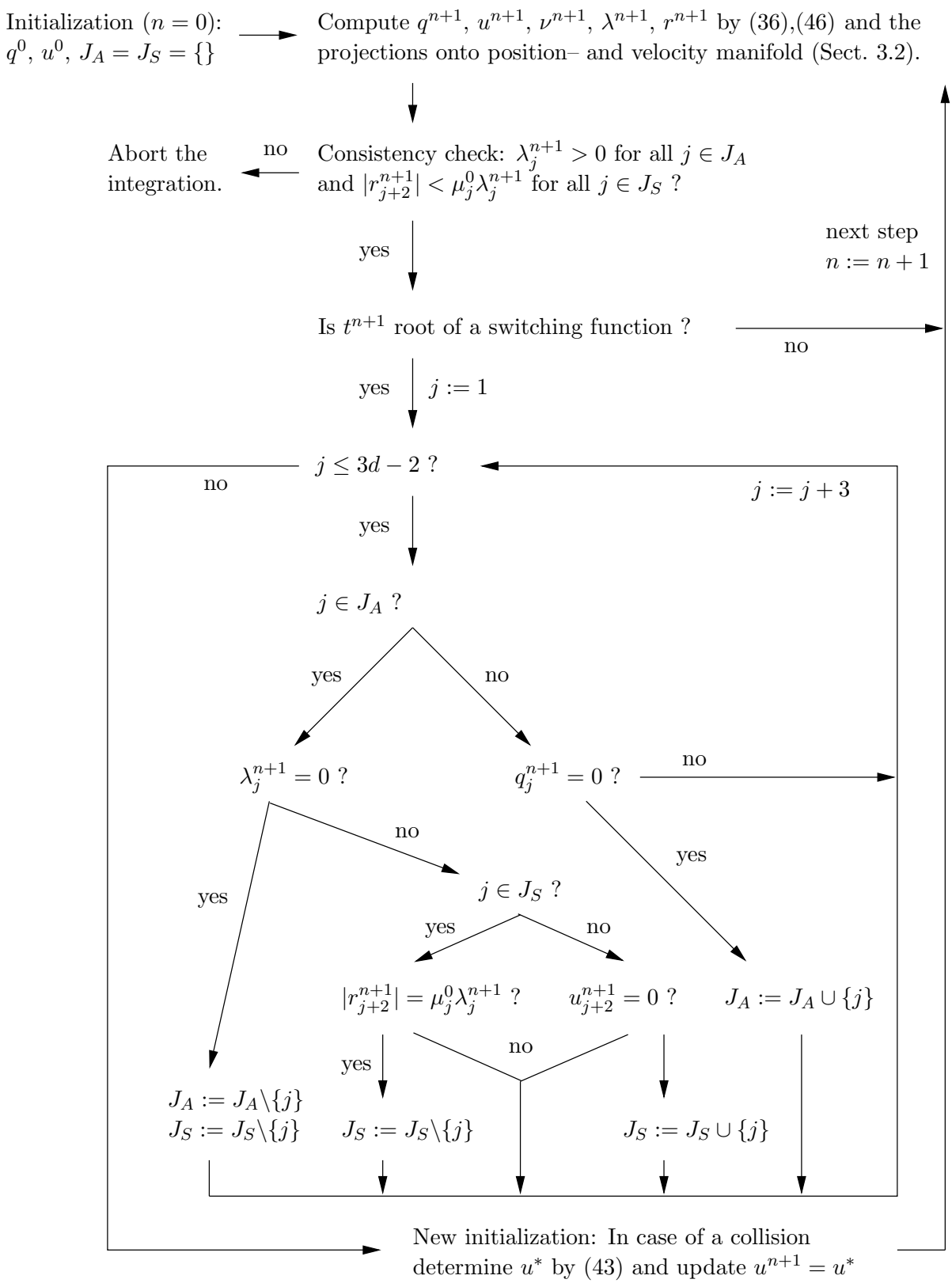

Figure 3: The switching algorithm. For simplicity we omit the arguments of the active/passive/sticking sets.

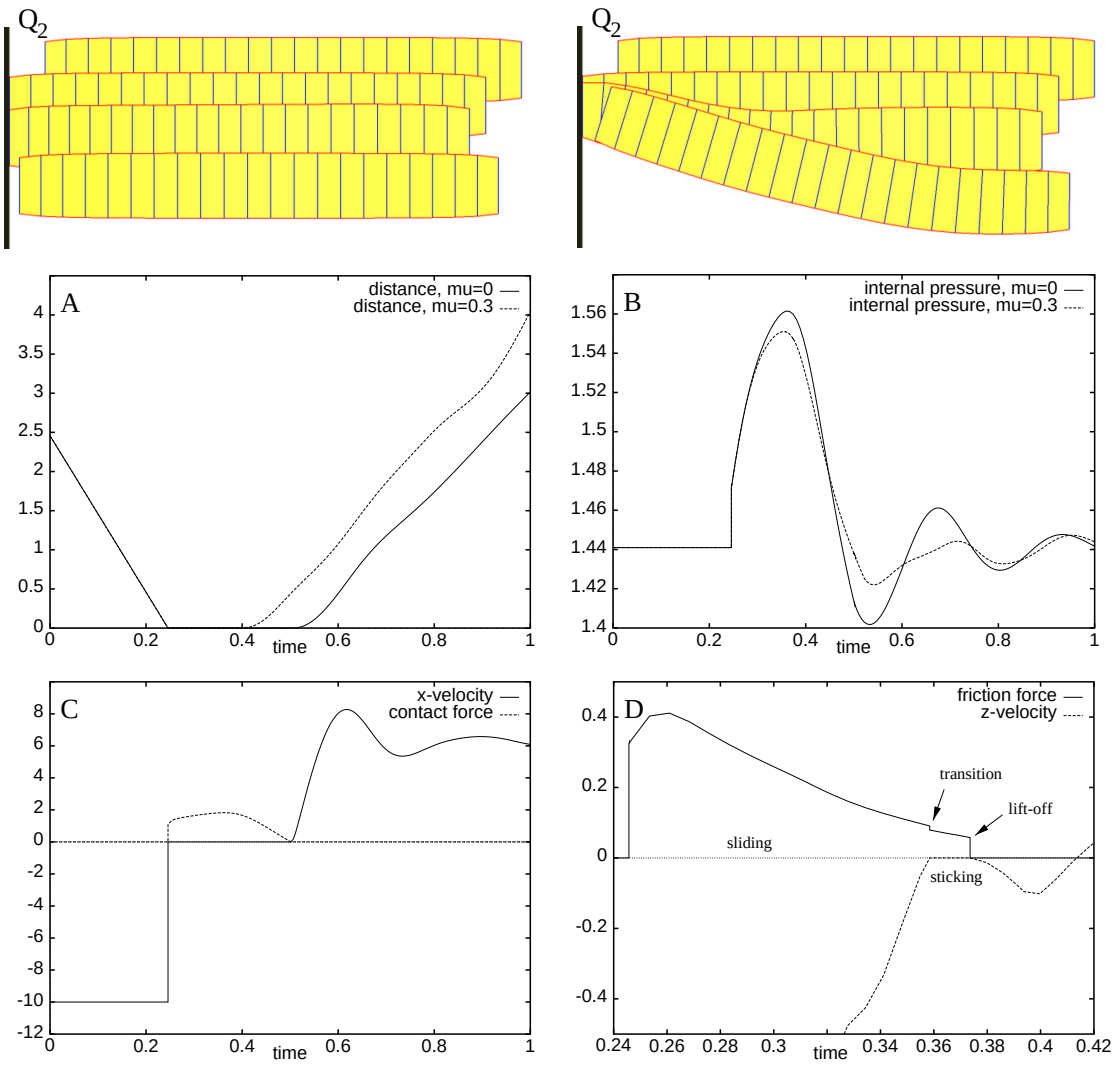

Figure 4: Collision of the non–compartmentalized model with the obstacle $\mathcal{H}$ in cases $\mu = 0$ (frictionless contact, left picture) and $\mu = 0.3$ (contact with tangential friction, right picture). We use Hooke's law combined with a linear damper (1),(2) for all elastic elements. The parameters of the LTCs in the steady state case are adapted to experimental data of the leech and the damping parameters are set to the value 0.1 as a first approximation. A: Distance of the corner Q_2 from the obstacle in both cases. B: Internal pressure in both cases. C: Velocity of the corner Q_2 in (horizontal) x–direction and contact force λ_2 acting on Q_2 in the frictionless case (for $\mu = 0.3$ we get a similar result). D: Velocity of the corner Q_2 in (vertical) z–direction and tangential friction force acting on Q_2 during both sliding and sticking.